Fermi National Accelerator Laboratory

FERMILAB-Pub-92/49

Hadroproduction of Charm Particles

J. Appel
Physics Department
Fermi National Accelerator Laboratory
P.O. Box 500, Batavia, Illinois 60510

February 1992

To appear in *Annual Review of Nuclear and Particle Science*, vol. 42, 1992.

Disclaimer

FERMILAB-Pub-92/49

HADROPRODUCTION OF CHARM PARTICLES

J.A. Appel
Fermi National Accelerator Laboratory
Physics Department
P.O. Box 500
Batavia, Illinois 60510

To appear in *Annual Review of Nuclear and Particle Science*, vol. 42 1992

TABLE OF CONTENTS

1. INTRODUCTION

The existence of the charm quark was postulated in 1970 by Glashow, Iliopoulos and Maiani to account for the absence of strangeness changing neutral currents (1). However, the first direct evidence for charm quarks came in 1974 from observations in a hadroproduction experiment at Brookhaven National Laboratory (2) and e^+e^- annihilations at the Stanford Linear Accelerator Center (3). These observations were the discovery of the J/ψ, a particle understood to be composed of a charm quark and charm anti-quark. The observations were rather quickly followed by measurements of higher mass quark-anti-quark states and open charm states, states with only a single charm quark or charm anti-quark in them. Identification of the J/ψ with the charm idea was quick. In time, evidence built that the constituents of the J/ψ were indeed strongly interacting quarks. However, in the dozen years after the very first observations of charm, hadroproduction played a limited, often confusing role.

1.1 Recent Progress

In the last five years the situation has improved. The charm results from hadroproduction experiments at CERN and Fermilab have become cleaner, less biased and have much higher statistical precision (e.g. Figure 1). These characteristics of recent experiments justify labeling them as a second generation of charm hadroproduction experiments. This second generation is the focus of this review. It is marked by precision measurements of the trajectories of charged particles coming from the production point and decay vertices of the charm particles. In addition, we can recognize the beginning of a third generation of experiments in which hadroproduction contributes to the detailed study of the decays of charm particles. This development arises as a continuation of the production studies which have demonstrated the ability to produce copious quantities of cleanly reconstructed charm decays. Meanwhile, we continue to expand on spectroscopy and other elements of the second generation of hadroproduction experiments.

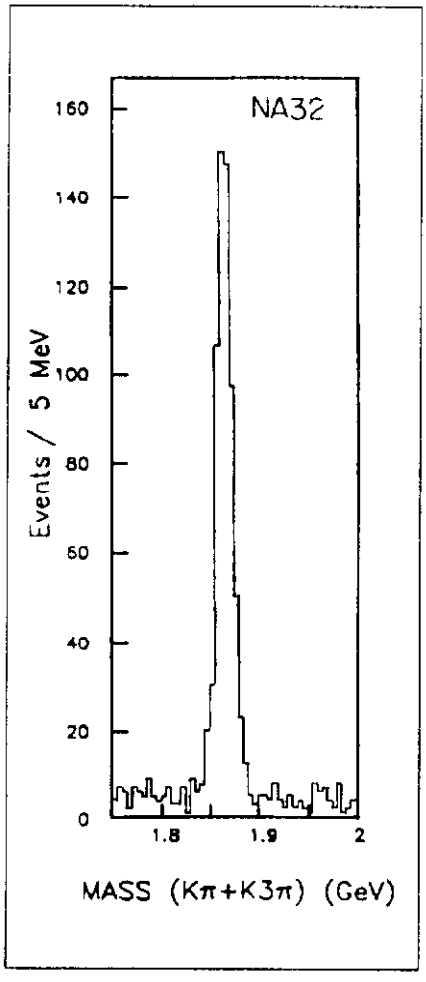

Figure 1. Effective mass spectrum of D^0 candidates from NA32 showing the benefits of precision tracking and decays in free space.

There has been similar recent progress in theoretical calculations. The quantum chromodynamic (QCD) next to leading order contribution to charm hadroproduction is available. The agreement of these calculations with the experimental cross-section measurements has increased confidence in the ability to interpret charm results in terms of this accepted theory. The calculations include differential cross-sections for inclusive processes and, most recently, next to leading order calculations including correlations between the pairs of charm particles produced.

1.2 The Physics of Charm Hadroproduction

Three basic elements enter the calculation of the hadroproduction process as understood by QCD. These are 1) a basic hard scattering between two constituents of the incident hadrons, 2) the distribution of those constituents inside the incident hadrons and 3) the hadronization of the produced charm quarks in which they become the charm particles observed in the laboratory.

In the hard scattering subprocess, one applies the universality of the QCD theory, coupling charm quarks in the same way as lighter quarks. The process is dominated at fixed target energies by gluon-gluon fusion. This provides the opportunity to study gluon physics in a rather well defined environment. Dependence on the distribution of gluons in the incident hadrons provides a method of studying the gluon structure function in a variety of particles. Beams of pions, kaons, protons and their anti-particles have been used in experiments, and these particles can have their gluon structure explored in this way.

Finally, as the charm quarks emerge from the hard production subprocess, they must pass through whatever residual hadronic matter there is locally, whether from the target or projectile. Since the formation time for the charm particle is comparable to nuclear distances, one may view the charm quark as traveling through nuclear matter for much of its "separate" existence. This provides an opportunity to probe yet another area of physics.

The wealth of physics processes involved in the hadroproduction of charm is both a benefit and a problem. The complexity of the full process allows for multiple interpretations of effects. Extracting parameters of the most basic physics quantities requires convolutions and other calculations which depend on the quantitative inputs as well as on the basic theory. On the more purely theoretical level, there are also parameters which are less well known than one would like for interpretations of the physics. Furthermore, there is the uncertainty due to the smallness of the charm quark mass. Is it heavy enough that perturbative QCD calculations can be used, even including next to leading order contributions, to extract the physics of interest?

1.3 Relation to Other Processes

The production of charm quarks at fixed target energies is a source of copious interactions where gluons interact in an identifiable way, i.e., the gluon-gluon fusion process. At hadron collider energies gluon splitting is an increasingly important source of charm quarks.

The gluon fusion events provide a tool for directly determining the gluon distribution in the incident hadrons. These structure functions are also relevant in lepton, photon and neutrino production of heavy quarks. In these processes, the gluons occur only in the target nucleons. The gluon structure function is obtained in deep inelastic scattering as a part of the evolution of the quark structure functions, i.e., as a correction to the dominant quark scattering. In direct photon production, gluons can enter directly, becoming quite large for some parts of the production. Nevertheless, subtractions due to quark sources are necessary. In

charm hadroproduction, the quark-anti-quark annihilation background is at most only on the order of 10% in leading order.

The hadronization of the charm quarks is among the least explored parts of the hadroproduction of charm. Hadronization occurs, of course, in any process in which the charm quarks are created. Fragmentation functions are a measure of this process. The most precise measure of hadronization comes from e^+e^- annihilations producing charm quarks. However, the environment of e^+e^- annihilation is different from hadroproduction. It is uncomplicated by the spectator hadronic matter which exists in hadroproduction.

Finally, hadroproduction is a copious source of particles containing the charm quark. As such, hadroproduction is already beginning to contribute to studies of the physics of heavy flavor decay. This role is likely to continue and expand. This aspect, however, will not be part of this review.

2. BRIEF HISTORY OF MEASUREMENTS

The early years of open charm hadroproduction were limited by the capability of detectors in the face of difficult experimental conditions. These conditions can be summarized as due to 1) the small fractional charm production cross section (1 charm pair event per 10^3 interactions, typically), 2) the large number of particles in the charm events and 3) the small branching ratios to the largest specific final states (typically 1-10%). As it turned out, many of the more reliable early measurements were indirect. Among these were the observations of prompt leptons which resulted from the semi-leptonic decays of charm particles. Most such early experiments had goals other than charm as their primary motivation. Nevertheless, the leptons in the intermediate transverse momentum range have been understood to come from charm. Charged leptons (electrons and muons) were found to occur at 10^{-4} and 10^{-3} of the pion rate at fixed target and collider energies, respectively. Muons and neutrinos were also measured in beam dump experiments where the beam dump had a variable density. All of these indirect measurements had large extrapolations from the observed lepton rate to those

which were produced "promptly" (i.e. directly or resulting from the decay of particles whose lifetimes were much less than those due to the weak decay of strange particles).

More direct measurements of charm decays resorted to limited regions of phase space. These were typically in the very forward direction or at high transverse momentum where there is better than the 1 part charm in 1000 which is characteristic of the charm cross section relative to the total cross section. Alternately, specialized cuts were chosen to select specific production or decay characteristics. Such techniques ordinarily did result in charm signals, but required very large extrapolations to go from the observation to physics parameters of interest. One even required multiplication by factors as large as 10^6 to go from observed signals to total cross-sections.

The experimental difficulties above led to many strange and controversial results and interpretations. The various results and attempts to understand them are well described in the excellent reviews of these early days by A. Kernan and G. VanDalen (4), and by S. Tavernier (5). The observational difficulties led to discrepancies of factors up to 100 in total cross sections and steep, even unimaginable energy dependence in going from fixed target ($\sqrt{s}$ in the range 17-39 GeV) to ISR collider energies ($\sqrt{s}$ of 53-62 GeV). Longitudinal momentum distributions suggested very strong leading particle effects, effects where charm particles having a quark in common with the incident beam particle were seen to dominate in the forward direction. Power law behaviors for longitudinal momentum distributions appeared to have powers which could vary by experiment and final state from 1 to 11. The average transverse momentum, p_t, of observed charm particles varied from 0.5 to 1 GeV. Some experiments did not see the major signals reported by other experiments with similar detectors. Mass distributions of a given charm particle peaked at different values in different data sets or even appeared to have double peaks. Attempts to explain the plethora of conflicting results were unavailing.

More recent experiments have benefited enormously by the application of new technology. Key among these are the techniques which provide sufficiently improved spatial resolution to "see" the decay of charm particles separated from their production point. As described in Section 4, the application of these techniques very much improved signal to background ratios. These, in turn, have allowed for charm measurements with full forward acceptance and more open triggers. Additionally, much greater on-line and off-line computing capabilities have lead to data samples which resulted in thousands of decays in an experiment instead of a few tens of decays. While results from the lower statistics efforts of this new generation continued some earlier confusion, more recent results have had much greater agreement among experiments, with less controversial and easier interpretations. This review, therefore, is based on a more coherent picture of charm hadroproduction, one in which the theoretical ideas are amenable to test and measurement results can provide input to further theoretical calculations.

3. BRIEF HISTORY OF THEORY

Theoretical efforts during the first generation of charm hadroproduction experiments were focused on explaining the conflicting early data. Quantum chromodynamics calculations, done to leading order at the time, fell short in explaining the cross-section and were unable to explain many features of the measurements. An uncomfortably low charm quark effective mass of 1.2 GeV was required to explain even the lowest of cross-section measurements. This left the field open to unconventional possibilities to explain the bulk of the charm data. These possibilities included intrinsic charm quarks existing in hadrons (6), excitation of more virtual charm quarks (7, 8), forms of diffractive production as analogs of the vector meson dominance model for photoproduction (9), and various enhancements (10) associated with the fragmentation or hadronization process as the partons of the basic interaction turn into the hadrons observed in the laboratory.

Coincident with the improved data of the second generation of hadroproduction experiments came complete QCD calculations in next to leading

order (11). These calculations indicated a nearly constant factor of three increase in cross section over the cross sections calculated to leading order in QCD. A more natural charm quark effective mass near 1.5 GeV was adequate to explain the total cross section. The success of these calculations and the lack of confirmed disagreement with them has removed the impetus to look for unconventional sources of charm or beyond the basic QCD theory. More details of the current theory of charm hadroproduction are given in Section 5 of this review.

4. DISCUSSION OF TECHNIQUES

The second generation of charm hadroproduction experiments is distinguished from first generation experiments by their ability to identify, by tracking alone, those particles which come from the decay of the charm particle. These particles are separated from all other particles in the event, the others from the production point and from the decay of the other charm particle. This capability has been provided by a high resolution small bubble chamber, emulsions and solid state detectors. These devices have been coupled to multiparticle spectrometers which serve to identify the produced particles, measure the momenta of the charged particles and generally select for further investigation those events which are most likely to have charm particles in them. In hadroproduction, so far, these techniques have only been applied in the fixed target environment.

4.1 Precision Tracking

Two important advantages result from the ability to reconstruct the trajectory of charged particles with high precision. The first advantage is the selection of events which have decays characterized by charm particle lifetimes, and therefore, are events highly enriched in charm relative to average events. Another large effect in improving signal to background comes in reducing the possible combinations of particles which need to be examined to find the charm. Hadronic interactions which produce charm are characterized by higher multiplicity than average events. Selecting only the trajectories of particles which come from a well

defined vertex reduces the number of combinations enormously. Only particles whose tracks form a good, separated decay vertex are considered. Overall background reductions by factors of hundreds are achieved. Efficiencies for the remaining charm, i.e., those whose lifetime in the laboratory allow seeing the decay vertex separately, can be as large as 50%, depending on the spatial resolution and particle proper lifetime.

Table 1 provides a comparison of the charm hadroproduction experiments of the second generation. Experiments prefixed by NA and WA for North Area and West Area are from CERN while those with an E are from Fermilab. A very large increase in the number of recorded events and in the number of reconstructed charm decays is evident in the table. Within the second generation of experiments, the spotlight has shifted from visual techniques associated with the bubble chamber and emulsion to purely electronic detectors. These later techniques provide the capability of very large statistics. The large statistics, in turn, have reduced the false observations due to statistical fluctuations and inability to adequately study backgrounds. These problems plagued the first generation experiments and even the early second generation experiments.

4.2 Downstream Spectrometers

Whatever the precision tracking device near the target, all second generation experiments have multi-particle spectrometers downstream. A typical example, that from the Tagged Photon Laboratory at Fermilab, is shown in Figure 2. It is characteristic of the other spectrometers in having charged particle tracking through magnetic fields and charged particle identification through two or more threshold Cerenkov counters or a ring imaging Cerenkov counter. Electron, photon and muon identification is achieved with electromagnetic calorimetry and with an absorber for filtering out non-muon charged particles.

The precision tracking provides spatial resolutions near the target ranging from a few to 20 microns. This is at least an order of magnitude higher precision than available in the proportional wire chambers or drift chambers used for the

Table 1 Experiment comparisons

Identifier	LEBC-EHS		LEBC-MPS	Hybrid Emulsion Spectrometers	
Experiment Number (reference)	NA27 (12)		E743 (13)	WA75 (14)	E653 (15)
Beam	360 GeV π^-	400 GeV p	800 GeV p	350 GeV π^-	800 GeV p 600 GeV π^-
Target			H_2	Emulsion	Emulsion
Year data taken	1982	1984	1985		1984-5 1987-8
# Si Planes Beam	2	2	0	6	6
Downstream	0 (LEBC)	0	0 (LEBC)	10	18
Resolution	2.5 μ	2.5 μ	2μ	20μ	5μ
#DC/PWC planes	66+ISIS	66+ISIS	24	49	55+12
ΔP_t MeV/c			700	900	336
Hadronic part. ID	TRD + 2$\check{C}$	TRD + 2$\check{C}$	TRD + 2$\check{C}$		TOF
($\check{C}$ or TRD) pion thresholds for $\check{C}$	.56, 17	.56, 17	5.7, 16.7		
EM calorimeter	$10-15\%/\sqrt{E}$	$10-15\%/\sqrt{E}$			$15\%/\sqrt{E}$
Hadron calorimeter	$150\%/\sqrt{E}$	$150\%/\sqrt{E}$			$80\%/\sqrt{E}$
μ ID	—	—	not used	2mFe+2mW	5m Fe
Trigger	interaction $n_{ch}>2$	interaction $n_{ch}>2$	interaction $n_{ch}>2$	muon $n_{ch}>3+\mu$	muon
Data sample size ($x10^6$)	0.115	1.0	0.5	1.5	5.4 9.6
Reconstructed charm	183†	425†	114†, 30	288†	146 ~1000

Identifier	ACCMOR			Omega		TPL	
Experiment Number (reference)	NA11 (16)	NA32 (17, 18)		WA82 (19)		E769	E791 (20)
Beam	175 GeV π^-	200 GeV π^-Kp	230 GeV π^-	340 GeV π^-	370 GeV P	250 GeV h±	500 GeV π^-
Target	Be	Si	Cu	Si, W, Cu,W	Cu, W	Be, Al, Cu, W	C, Pt
Year data taken	1982	1984	1986	'87-88-89	'89-88	1987-88	1991
# Si Planes Beam	6	7		8		2	6
Downstream	6	7	8 + 2 CCDs	13+1		11	17
Resolution	6μ	5-8μ		10μ		20μ	
#DC/PWC planes	48	48		~6		37	
ΔP_t (MeV/c)	270.7 +617.4	270.7 +617.4		2190		525	
Hadronic part. ID	3$\check{C}$	3$\check{C}$	2$\check{C}$	RICH	—	2$\check{C}$	
($\check{C}$ or TRD) pion thresholds for $\check{C}$	12 GeV	2.4, 6.1, 12.8	6.5, 12	in '87-88		6, 10.5	6, 11
EM calorimeter	$18\%/\sqrt{E}$	$18\%/\sqrt{E}$	None	$15\%/\sqrt{E}$		$20\%/\sqrt{E}$	
Hadron calorimeter	None	None		None		$75\%/\sqrt{E}$	
μ ID	None	None		None		2m Fe	
Trigger	Single electron	Interaction	a pair of K or p of opposite sign	Impact parameter		Global E_t $n_{ch}>5$	$n_{ch}>4$
Data sample size ($x10^6$)	6.3	3.8	17	18 + 30	10	500	20,000
Reconstructed charm	130	170	~1300	~3,000		~4,000	(>100,000)

† topological only
() anticipated

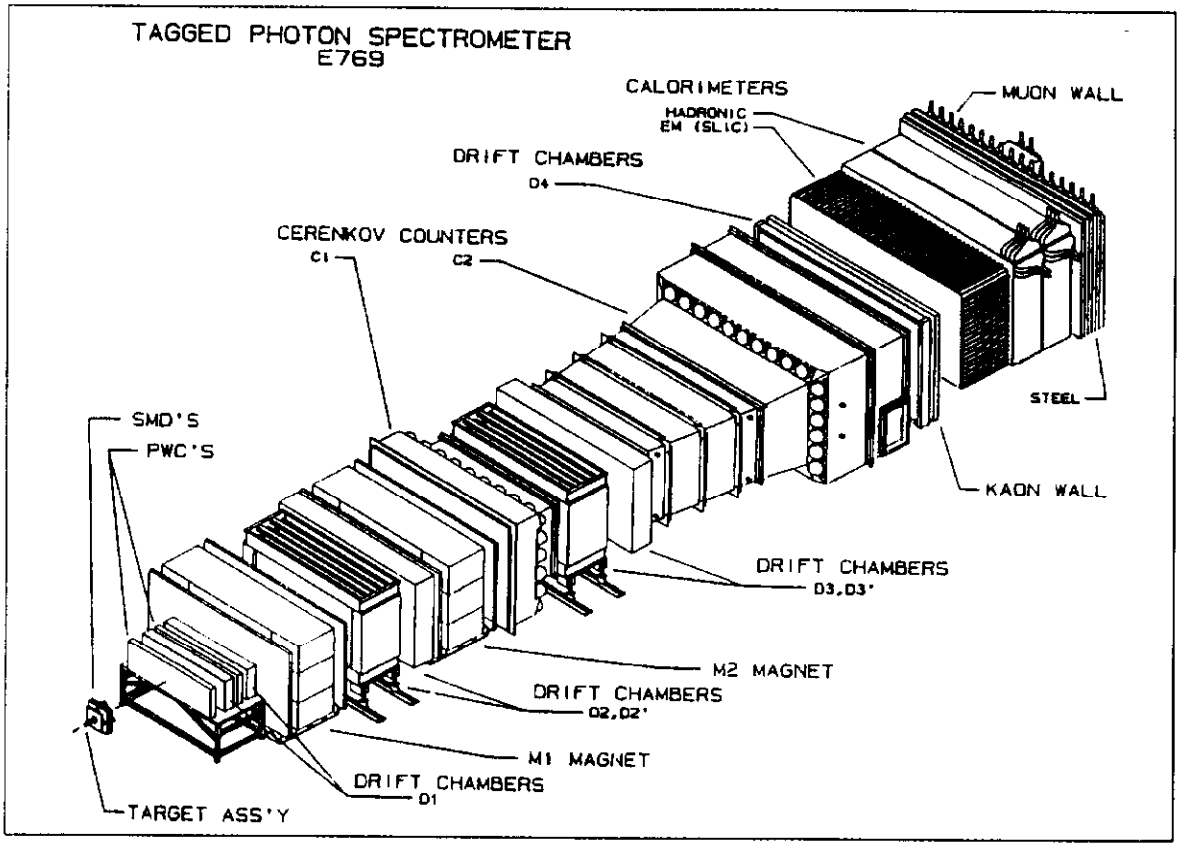

Figure 2. The Fermilab Tagged Photon Spectrometer, a typical fixed target multi-particle measuring apparatus.

more downstream tracking. On the other hand, the physical extent of the precision tracking is only a few centimeters. The wire chamber chambers used for downstream tracking extend over at least ten meters. This results in comparable angular resolution in the downstream tracking to that achieved with the higher precision tracking near the target. Thus, wire chamber tracking has poor position resolution compared to solid state devices, but comparable angular resolution.

The limited spatial extent of the precision trackers limits the size of the useful target. Thus, these experiments all have small luminous regions for targets, even in the direction parallel to the incident beam. There are no long liquid hydrogen targets, and all of the experiments with solid state detectors use thin targets to maintain large forward solid angle acceptance. This increases the importance of measurements of the dependence on the target material. One sees a variety of targets in each of these experiments.

4.3 Selecting Events Containing Charm

The small fractional probability of producing charm remains a technical problem for experiments. One must still sift through enormous numbers of events before finding those which have the charm particles. This selection is done by some combination of triggering at the time the data are taken (on-line) and is typically extended in the analysis made later (off-line).

The need to sort through large numbers of interactions to find the sought after signals has lead to a variety of solutions (21). While the bubble chamber has limited its event recording to events in which beam particles create interactions in the bubble chamber, all other experiments have used even more restrictive triggers. The emulsion experiments demanded a high transverse momentum muon downstream to flag potential charm containing events. The experiments with solid state detectors have used triggers based on particle identification in the downstream spectrometer (electrons, muons and kaons or protons), evidence for secondary vertices or downstream decays and global transverse energy. Each of these help select events where the fraction of charm is higher than in a random sampling of interactions.

As one has learned from off-line analysis how to select the charm events, the lessons have moved upstream into the data taking itself. Fast processors with exotic names like ESOP (22), FAMP (23) and MICE (24) have been used in CERN hadroproduction experiments. These specialized processors have calculated electron identification probability and evidence for downstream decays, for example. The results enter the decision on whether to write the event to magnetic tape for later analysis. An alternate approach has been pursued at Fermilab where networks of microprocessors have been assembled for rapid reconstruction of larger data sets off-line. This approach has allowed looser on-line requirements, but has also required faster event readout time to achieve the sample sizes currently taken. One experiment (E791) recorded 20 billion events onto 8 mm tapes. This required faster digitization and readout of front end electronics and

significant parallelism in the data acquisition system. An average sized event could be read out in 35 microseconds. This is much faster than any of the processor systems used so far at CERN could make a decision on an event. That decision is pushed off-line in E791 to the massively parallel network of microprocessors organized in what are called "farms" (25). The farms are used for selecting which events will be fully reconstructed and then doing so.

4.4 Hadron Collider Experiments in the Future

Precision vertexing is now being added to the CDF hadron collider experiment (26) at Fermilab, motivated by tagging events containing bottom quarks as an aid in the search for top quarks. It is possible that CDF, and eventually other hadron collider experiments, will contribute to charm hadroproduction measurements in the future. Such contributions would be welcome since the kinematic range of production is very different from that in fixed target experiments. Additional processes such as gluon splitting may be explored as an different probe of QCD. Nevertheless, since the x regions explored are at very low values, theoretical interpretations are more difficult. They involve yet higher order processes and more non-perturbative effects. There are also significant technical difficulties in the added backgrounds for production so far from threshold (e.g., charm from bottom quark decay). Thus, hadron collider charm production measurements will presumably also begin by making measurements in limited regions of phase space, etc.

Without the precision vertexing and its capability for background rejection, collider experiments have been limited so far to measuring the fractional rate of D^* production. Using the small energy release in the D^* decay to D^0 plus a pion, both UA1 (27) and CDF (28) have reported that about 10% of jets contain D^*'s in the fractional momentum range where the D^*'s have at least 10% of the jet energy. As was characteristic of other first generation charm results, the UA1 result was changed from the value published by the same group five years earlier (29).

4.5 Other Attempts and Techniques

A wide variety of other techniques have been developed for use in charm experiments. The techniques have focused on precision reconstruction of the production and decay region. Holographic bubble chambers (30) and streamer chambers (31) have been developed. However, while these might enlarge the volume in which decays could be reconstructed with high resolution, the inherent cycle times of the devices make them uncompetitive today. Inherently faster devices based on bundles of scintillating fibers (32) have been tried at CERN and Fermilab. However, conversion of light images to digital format for recording and later analysis has added a technical problem, which, coupled to the sometimes marginal light output of the devices, has shifted attention from these techniques. Another technique tried at both CERN and Fermilab, actively read targets of silicon (33), has failed to achieve notable success. Here, variation in ionization by individual particles and signals due to target nuclear breakup have limited results. The main goal has been to see a multiplicity jump due to the decay of charm particles within the target region.

Solid state devices remain the favorite technique for recognizing and measuring trajectories of charged particles from charm decays. These devices are reviewed in this volume by Helmuth Spieler. Here, we simply note the preponderance of silicon microstrip detectors, arrays with one dimensional readout. While charged coupled devices (CCD's) have been used by the ACCMOR collaboration at CERN, their slow readout has prevented their wider use in spite of the advantages of the two dimensional readout and higher spatial resolution they provide. Efforts at greater integration of the readout electronics using modern microelectronic technology (34) may change this in the future. However, the enormous increase in the number of readout elements, already quite large for the microstrip detectors, provides a challenge, both for their use in fast trigger schemes and general readout.

5. QCD THEORY OF CHARM HADROPRODUCTION

The leading order QCD diagrams (i.e., schematic representations of the basic processes) for charm hadroproduction are shown in Figure 3. It is assumed that there is a hard scattering of one parton (quarks, antiquarks or gluons) from each of the incident hadrons. The hard scattering is necessary to produce the relatively high mass of the charm quark pair. The calculations are performed in this parton model starting with Equation 1.

$$\sigma = \sum_{ij} \int dx_1 dx_2 f_i(x_1,\mu) f_j(x_2,\mu) \hat{\sigma}\left(x_1 x_2 s, \mu^2\right) \tag{1}$$

In Equation 1, one begins with the distributions, f_i and f_j, of the relevant partons in the incident hadrons. These distributions are called structure functions, the number densities of the light quarks and gluons as a function of their momentum fraction, x_i and x_j, evaluated at a scale μ. The partons from the incident hadrons interact with the cross section, $\hat{\sigma}$, a function of the momenta of the incident partons and the scale μ. The total center of mass energy squared of the incident hadrons is s. The total center of mass energy squared of the partonic subprocess is $x_1 x_2 s$.

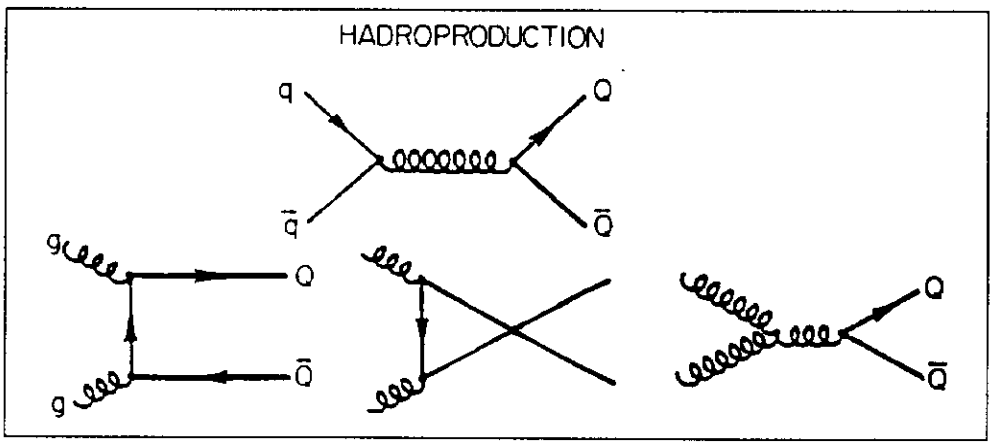

Figure 3. Leading order QCD diagrams for the hadroproduction of charm quarks, Q.

5.1 *QCD Perturbative Calculations*

The parton level cross section, $\hat{\sigma}$, is normally calculated in a perturbative series in the strong interaction coupling constant $\alpha_S(\mu^2)$. The use of Equation 1 for calculations ignores all of the possible effects discussed in Section 3. Flavor excitation is ignored, as is the role of the spectator (non-interacting) non-charm producing partons in the incident hadrons. This leading order cross section is proportional to α_s^2. These first order calculations have been done by a number of authors (35) and the justification of the factorization represented by Equation 1 examined on the basis of the lowest order contributions (36).

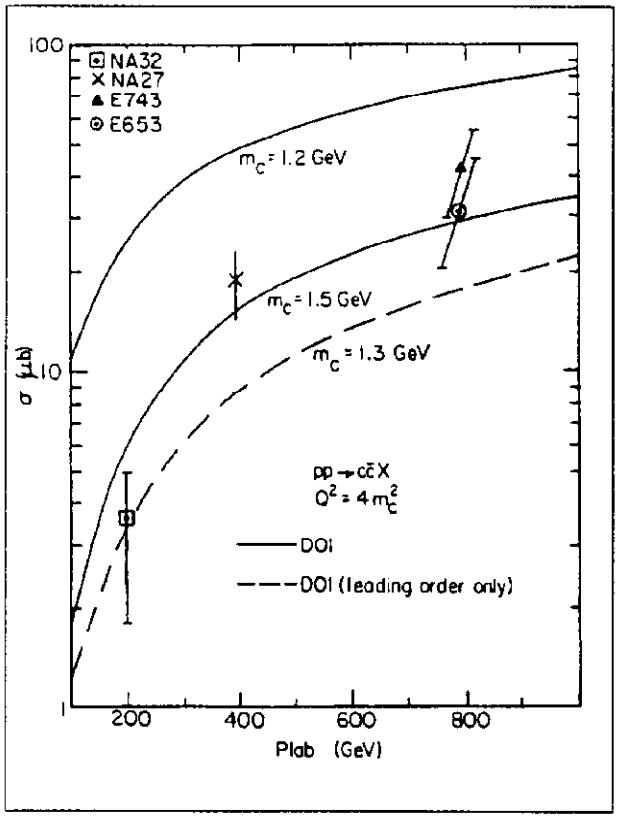

Figure 4. Total charm quark production vs incident proton momentum. The dashed curve represents a calculation to leading order only with a charm quark mass of 1.3 GeV. The two solid curves represent calculations in next to leading order with the indicated charm quark masses.

More recent calculations by Nason, Dawson and Ellis (11, 37) and Beenakker, et al (38) provide a complete next to leading order calculation of $\hat{\sigma}$. In this calculation, a great many additional diagrams are included. The cross section goes as the square of the sum of the amplitudes represented by these diagrams and terms proportional to α_s^3 are kept. The net result of these calculations is that the total cross section increased by a factor of about 3 relative to the leading order calculation. Agreement with the total cross section data is comfortably achieved with charm quark masses on the order of 1.5 GeV as seen in Figure 4 (39). Differential cross section shapes do not change much by the addition of the next to

leading order diagrams. There is still no intrinsic charm quark included in the calculations, but diagrams having the same topology as flavor excitation (Figure 5) (8) are included in these higher order calculations.

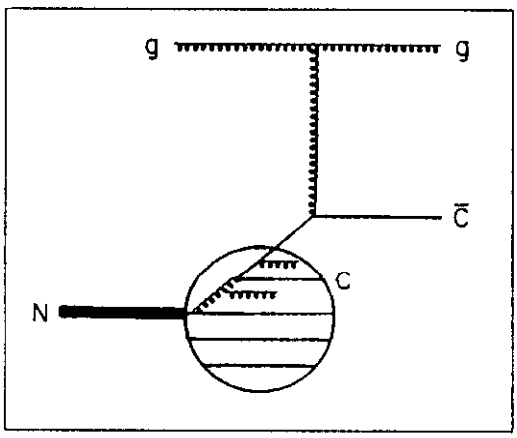

Figure 5. Charm quark excitation diagram from Odorico (8).

Given the large increase in rate provided by the next to leading order calculation, one might ask whether the next order terms are negligible. In addition, there are significant uncertainties remaining in the predictions of these theoretical calculations. These include the precise values of the effective mass of the charm quark, and the renormalization scale. There are also effects associated with the spectator partons, etc. of the order of Λ/m_c (the strong interaction scale over the mass of the charm quark). In spite of these uncertainties, the QCD framework provides a useful tool in understanding the process itself. Furthermore, comparisons involving different incident hadrons and outgoing charm particles may be expected to have common basic interaction calculations and high order calculations even if these cannot be performed explicitly. It may be useful to see how far one can pursue application of the current theory.

5.2 Structure Functions

So far, gluon and quark structure functions have been taken as input to calculations of charm production. These inputs come from compilations of data on deep inelastic lepton scattering and neutrino interactions. This is particularly appropriate for the nucleon's quark structure functions where the data are easier to interpret and more precise. However, the gluon structure function is not well determined. In the case of pions and especially kaons, the gluon structure function is essentially unmeasured. One may anticipate that the best informa-

tion on these structure functions will come from analysis of the high statistics production data coming from the second generation hadroproduction of charm experiments, especially the energy dependence of the cross section and the longitudinal momentum dependence of charm particles. Uncertainties associated with the perturbative calculations above and the hadronization process described below will affect the absolute determination of structure functions. However, comparisons of pion and kaon production of charm on the same target should allow determination of the relative hardness of their gluon distributions. Does the extra mass of the strange quark influence the gluon distribution of the kaon relative to the pion? Similarly, the gluon distributions in the quark-antiquark mesons may be different from the gluon distributions in the three quark baryon. Such comparisons are of basic interest and provide relevant tests for lattice gauge calculations.

5.3 Fragmentation / Hadronization

The calculations described so far relate to the inclusive production of charm quarks. The development of these quarks into charm hadrons requires additional, non-perturbative calculations. These are normally represented by fragmentation functions which, one might hope, would be the same as those measured in e^+e^- annihilation into charm quarks. However, the direct applicability of these functions is not apparent.

The fragmentation has not been calculated as extensively or analytically as the quark production itself. Monte Carlo style calculations are more typical of theoretical efforts. Three models dominate the efforts at this time. These are: string fragmentation, cluster fragmentation and independent fragmentation. The status of these fragmentation models has been reviewed recently by T. Sjöstrand (40). The Monte Carlo calculations are used widely by experimentalists in modeling the physics presented to their detectors. Well known and widely available Monte Carlo programs such as ISAJET (41), PYTHIA (42) and EUROJET (43) are used. The focus of these programs has been on collider energies and, in

fact, none of the physics generators of these or other programs have been tuned to match the results of fixed target charm production. ISAJET uses an independent fragmentation model (44) while the others, LUND programs, use JETSET which is based on string fragmentation. FRITIOF (45), the newest member of the Lund family, is more relevant for fixed target experiments. It is aimed at hadron-nucleus collisions and pays more attention to the spectator partons in events.

6. RECENT DATA ON INCLUSIVE CHARM HADROPRODUCTION

The three physical quantities describing the inclusive production of charm particles are the total cross section, the longitudinal momentum distribution and the transverse momentum distribution. The longitudinal momentum distributions are usually parameterized in terms of the Feynman x, x_F. This is the longitudinal momentum in the center of mass divided by its maximum value:

$$x_F = \frac{p\,(\text{parallel to the incident beam})}{p\ \text{maximum}} \tag{2}$$

Data on correlations between the two charm particles produced in an event are discussed in Section 7. The dependence of results on the nuclear target material is discussed in Section 8.

6.1 Total Cross Section

Recent data on the total cross section for the proton induced interactions has already been shown in Figure 4. The recent data (Table 2) can be easily modeled with the QCD predictions including next to leading order contributions and using a charm quark effective mass of about 1.5 GeV. This fits both the absolute cross section and the energy rise from 400 to 800 GeV. There are more experiments on charm production by incident mesons, but the energy range is still small for those who have reported on the total cross section. More results with a broader incident

Table 2 Recent open charm cross section data

Exp't	Particle	# Events	σ or σB $x_F>0$ μb/nuclear	ref.
NA32	D^0	543	$\sigma = 6.3\pm0.3\pm1.2$	(46)
π^-	D^+	249	$\sigma = 3.2\pm0.2\pm0.7$	
230 GeV	All D	792	$\sigma = 9.5\pm0.4\pm1.9$	
	$D_s \to KK\pi$	60	$\sigma B = 0.067\pm.011\pm.010$	
	D^*	147	$\sigma = 3.4\pm0.3\pm0.8$	
	$\Lambda_c \to pK\pi$	154	$\sigma B = 0.18\pm.02\pm.03$	(47)
			$R(\Lambda_c/\overline{\Lambda}_c) = 0.99\pm.16$	
	$\Xi_c^0 \to pKK^*(892)$	3	$\sigma B = 0.019\pm.011\ ^{+.066}_{-.009}$	(48)
	$\Xi_c^+ \to \Xi^-\pi^+\pi^+$	3	$\sigma B = 0.13\pm0.08\ ^{+.07}_{-.05}$	(49)
	$\Xi_c^+ \to \Sigma^+K^-\pi^+$	2	$\sigma B = 0.012$	(49)
E769	All D	2283	$\sigma = 9.1\pm2.1\pm1.2$	(50)
π^-	$D_s \to \phi\pi + K^*K$	29	$\sigma B = 0.036\pm0.015$	(51)
250 GeV				
NA32	All D	31	$\sigma = 8.5\pm1.6\pm1.2$	(46)
K^-			$(K^-N \to D/\pi^-N \to D) = 0.9\pm0.2$	(46)
230 GeV				
	$D_s \to KK\pi$	4	$\sigma B = 0.11\pm0.06\pm0.02$	(46)
	Λ_c	7	All $\overline{\Lambda}_c$!	(47)
	Ξ_c^0	1		(48)
	Ξ_c^+	1		(49)
NA32	All D	9	$1.5\pm0.7\pm0.1$	(52)
P				
200 GeV				
E653	$c,\bar{c}$ (from D^0)	146 + 35	$38\pm3\pm13$ μb	(53)
p	$c,\bar{c}$ (from D^+)		$38\pm9\pm14$ μb	
800 GeV			All x_F	

energy range should be available soon. However, the size of the pion and kaon production cross sections appear to be larger than that for protons at the same incident momentum, consistent with a harder gluon distribution in the mesons.

6.2 *Longitudinal Momentum Distributions*

The longitudinal momentum distribution is conventionally fit to the form in Equation 3

$$\frac{d\sigma}{dx_F} \propto (1 - x_F)^n \tag{3}$$

This form was motivated historically by kinematic considerations at high x_F, and there are predictions by Gunion (54) for the power n at high x_F. Nevertheless, the form appears to fit the data down to quite low values of x_F. Most of the new experiments have significant acceptance only for $x_F > 0$. Although the theory predicts a maximum somewhat forward of $x_F = 0$ for mesons, data are not yet sufficiently precise to distinguish this offset. Figure 6 (50) is an example of the scaled longitudinal momentum distribution and a fit (solid line) to the above form. A single contribution with this functional form seems to fit the data over two orders of magnitude. There is no evidence for 10-20% of the total cross section having a second x_F distribution as reported earlier (55).

Figure 6 also shows two theoretical curves. The dashed line is taken from the first order calculation of Nason, Dawson and Ellis (37) and comes quite close to fitting the data. The normalization has been floated in this fit. Since the calculation is done for charm quarks, the fragmentation process would have to be such that the charm particle takes all the momentum of the charm quark (a δ function for fragmentation!). Using fragmentation functions from e^+e^- annihilation reduces the average x_F. A convolution of one such fragmentation function with the theoretical prediction for charm quarks is shown by the dotted line in Figure 6. This simple convolution of fragmentation functions does not represent what happens in this data from hadroproduction on nuclear targets. It may be that the drag due to color strings attached to the opposite and residual spectator partons is balanced by a pull of other color strings towards spectator partons going

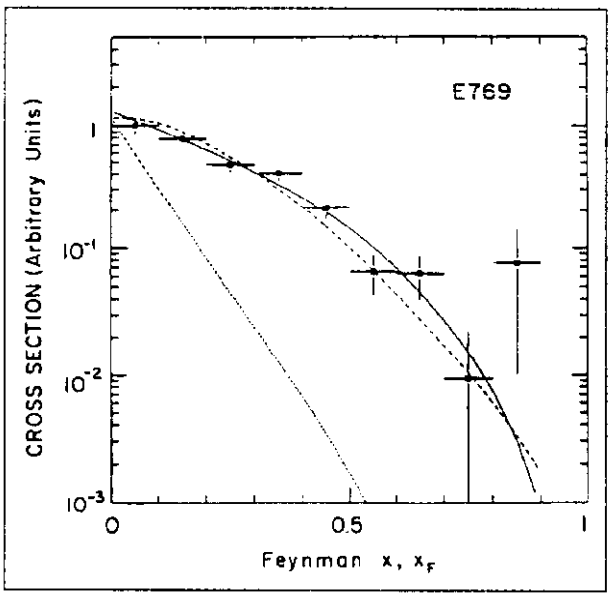

Figure 6. Scaled longitudinal momentum distribution of $D^{\pm}$ mesons. The solid curve is the best fit to the data using equation 3. The dashed curve is for charm quark production from (37). The dotted curve is this distribution convoluted with fragmentation functions from e^+e^- annihilations (50).

in the same direction as the charm quark. Such processes are included in the Lund fragmentation, but overestimate the leading particle effect (56).

All the pion and kaon induced charm data (Table 3) have the power law behavior of Equation 6 with the power in the range of 3 to 4. Protons at similar energy have a softer distribution corresponding to a larger n. There has been a suggestion that protons have an increasingly soft distribution with increasing energy. However, such an energy dependence is not well established in recent data nor explained by current theoretical calculations.

6.3 Transverse Momentum Distribution

The data on transverse momentum distributions (Table 3) now extend out to transverse momenta of 4 GeV. The data from WA82 (59), shown in Figure 7, and from E769 (50) which reach these p_t values suggest a simple exponential behavior beyond the lowest p_t. These experiments and previous experiments with smaller p_t range have traditionally fit their data with a Gaussian distribution as in Equation 4.

$$\frac{d\sigma}{dp_t^2} \propto e^{-bp_t^2} \tag{4}$$

The average p_t is measured to be approximately 1 GeV and is in agreement with QCD calculations which give average p_t's comparable to the charm quark mass.

Table 3 Recent x_F and p_t dependence data

Expt	Beam	Particle	n	b(GeV^{-2})	ref.
NA32	200 GeV π^-	All D	$2.5\pm^{+0.4}_{-0.3}$	$1.06^{+0.12}_{-0.11}$	(52)
		Leading D	$2.1\pm^{+0.5}_{-0.4}$	$1.22^{+0.20}_{-0.17}$	
		Non Leading	$3.3\pm^{+0.6}_{-0.5}$	$0.91^{+0.12}_{-0.11}$	
NA32	230 GeV π^-	All D	3.74±0.23±0.37	0.83±0.03±0.02	(46)
		Leading D	$3.23^{+0.30}_{-0.28}$	0.74±0.04	
		Non Leading	$4.34^{+0.36}_{-0.35}$	0.95±0.05	
		A_c	$3.52^{+0.51}_{-0.49}$	0.84±0.09	
		D_s	$3.94^{+0.93}_{-0.86}$	0.59±0.10	
E769	250 GeV π^-	$D^{\pm}$	3.21±.24		(50)
		Leading D	2.84±0.31		
		Non Leading D	3.50±0.36		
		D^0	4.2±.5	1.09±.15	(57)
WA82	340 GeV π^-	All D	2.9±0.1±0.3	0.78±0.04	(58)
NA27	360 GeV π^-	All D	3.8±0.6	1.18±0.17	(55)
		Leading D	$1.8^{+1.6}_{-0.5}$		
		Non Leading	$7.9^{+1.6}_{-1.4}$		
NA32	200 GeV K^-	All D	4.7±0.9	$2.7^{+0.7}_{-0.5}$	(52)
NA32	230 GeV K^-	All D	$3.56^{+1.08}_{-0.99}$	$1.36\pm^{0.32}_{0.26}$	(46)
WA82	370 GeV p	All D	5.5±0.8	1.27±0.18	(58,59)
NA32	200 GeV p	All D	$5.5^{+2.1}_{-1.8}$	$1.4^{+0.6}_{-0.4}$	(52)
NA27	400 GeV p	All c	4.9±0.5	1.0±0.1	(60)
E743	800 GeV p	All c	8.6±2.0	0.8±0.2	(61)
E653	800 GeV p	All c	$6.9^{+1.9}_{-1.8}$	$0.84\pm^{0.10}_{0.08}$	(53)
			$6.8^{+2.1}_{-1.9}$ $x_F > 0$		(53)
			$8.3^{+6.0}_{-5.6}$ $x_F < 0$		(53)

At high enough incident energy and p_t, there could be a small contribution from bottom quark decay to charm. However, neither the measurements of bottom production at these energies nor the statistics at the highest p_t values are sufficient to demonstrate such an effect. Both E791, the follow-on to E769 at Fermilab, and WA92, the follow-on to WA82 at CERN, may be able to address this possibility.

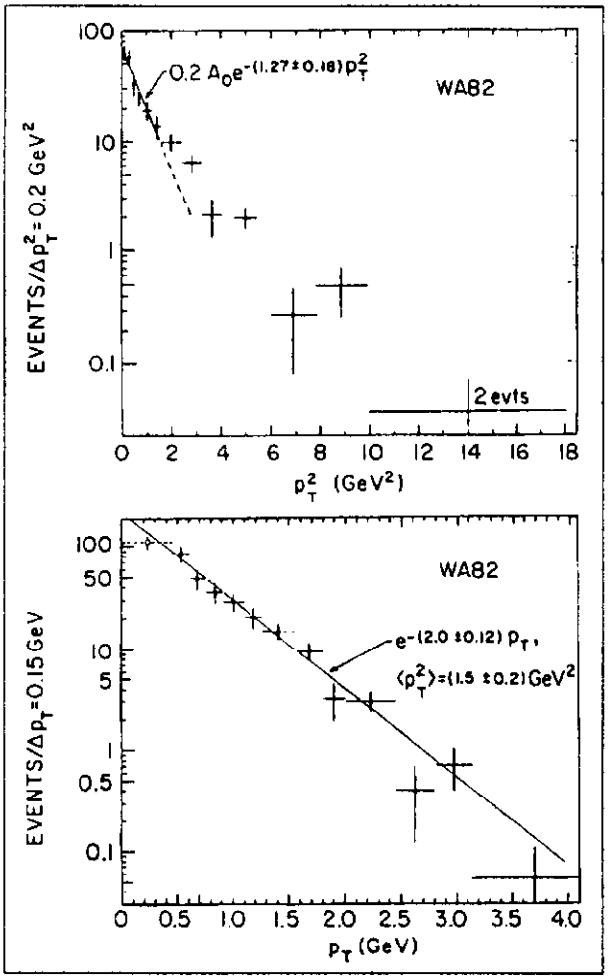

Figure 7. Transverse momentum distributions from WA82 for D mesons indicating the preference for a simple exponential fit at high transverse momentum.

6.4 Comparing Structure Functions

The total cross section and x_F dependence data is useful for comparing structure functions among mesons and protons. On the basis of what is known so far, it appears that the pion and kaon have similar gluon structure functions. The mass of the strange quark does not appear to change the gluon distribution dramatically. The three quark baryon has a softer gluon distribution (i.e., larger n).

6.5 Fragmentation to Specific Final States

In the simplest models with equal partition of energy among possible states and ignoring mass effects, one might anticipate charm final states appearing in proportion to the spin factor, (2J + 1). This would argue for equal numbers of directly produced D^+ and D^0, and a factor of 3 for each of the charged states of the D^*. The lowest mass baryon might have a factor of 2 larger production relative to the single charge pseudoscalar mesons. Beyond this, one might anticipate a factor of 10 to 20 reduction for each additional strange quark in the final state. Such a picture is grossly consistent with the data for the lowest mass states shown in Table 2. However, detailed quantitative statements require more analysis from the experiments and measurement of the absolute branching ratios of the baryons and charm-strange states. Again, it will be interesting to compare results here with the e^+e^- annihilation and photoproduction ratios.

7. CORRELATIONS IN PRODUCTION OF CHARM PAIRS

Observations of both of the charm particles produced in a hadron induced event hold promise for additional information on the production process and for tests of QCD. In addition, if the production dynamics are known, it is possible to determine absolute branching ratios for charm decays from such data.

Observations of pairs of charm particles in events fall into two classes. In the first class, the individual charm decays are identified by topological reconstruction in bubble chamber pictures (62, 63) or emulsion (64, 65). In the second class of observations, one reconstructs fully one or both final state charm decays using the more complete information from spectrometers. In the first class of observations, the efficiency for observing a second decay, given the first decay, is quite large, approaching 60-80% in published results. This high efficiency is important, of course, since the number of events with at least one charm decay is limited by the number of events which one can measure. In the second class of experiments, the number of double charm events is more typically 1% of the number of inclusive charm decays observed. This is due not only to the geometrical acceptance of the detectors (typically smaller by at least a factor of 2), but more so to the much smaller fraction of charm decays which can be fully reconstructed in the existing detectors. The much larger sample of inclusive charm, however, overcomes the branching fraction limitation. In addition, the use of fully reconstructed charm pairs allows the measurement of more precise physical quantities since both longitudinal and transverse momenta are explicitly measured. In the topological measurements, one must basically be satisfied with azimuthal correlations or heavy dependence on models for unfolding other kinematic correlations. Table 4 lists the recent experiments with published results on double charm events. So far, the physics results are scattered over a variety of topics. These include raw kinematic correlations, meson-meson and meson-baryon final state production ratios and qualitative tests of QCD with evidence for next to leading order processes.

Table 4 Charm correlations

Experiment	Energy	Beam/Target	Number Events	Physics Results	ref.
NA32	230	π^-/Cu	584	Final States	(66)
				Absolute BR's	(66)
				Angular Correlations	(66)
WA75	350	π^-/Emulsion	102	Final States	(64)
				Angular Correlations	(64)
LEBC-EHS	360	π^-/p	53	Angular Correlations	(62)
LEBC-EHS	400	p/p	233	Angular Correlations	(63)
E653	800	p/Emulsion	35	Angular Correlations	(65)

Angular correlations are the most copious results from the various experiments. The charm and anti-charm particles are expected to be opposite each other in the transverse plane in the simplest parton models. Only the intrinsic transverse momentum of the incident partons, k_T, modifies this. Indeed, opposite peaking (62-66) is observed. However, the width of the correlations are much broader than one predicts from leading order gluon fusion model calculations. This supplies evidence for the importance of next to leading order effects where emitted gluons would further modify the nearly back-to-back production of the final charm hadrons. In general, the peaking increases (e.g., as shown in Figure 8) with such kinematic variables as the mass of the charm pair, the transverse momentum of the charm pair and the rapidity gap of the charm particles (67). This is as one might expect in the hardest collisions, as tagged by high values of these parameters. On the other hand, E653 observes polar angle peaking which is more pronounced than predicted by QCD models.

NA32 has the largest pair sample with 642 charm pair events (only 584 of these appear to be charm-anti-charm). From the charm-anti-charm events, they report (66) a dominant fraction of pair produced charm ($D\overline{D}$ and $\Lambda_c\overline{\Lambda}_c$, etc.) relative to associated production ($D\overline{\Lambda}_c$ etc.). Among these events, the $D\overline{D}$ seem to be produced back-to-back in the plane perpendicular to the beam. The $D\overline{D}_s$ are not so, and the associated production seems to lie in-between. With their sample, they explore the technique of determining absolute branching ratios (68) and obtain (model dependent) results consistent with the more precise measurements from

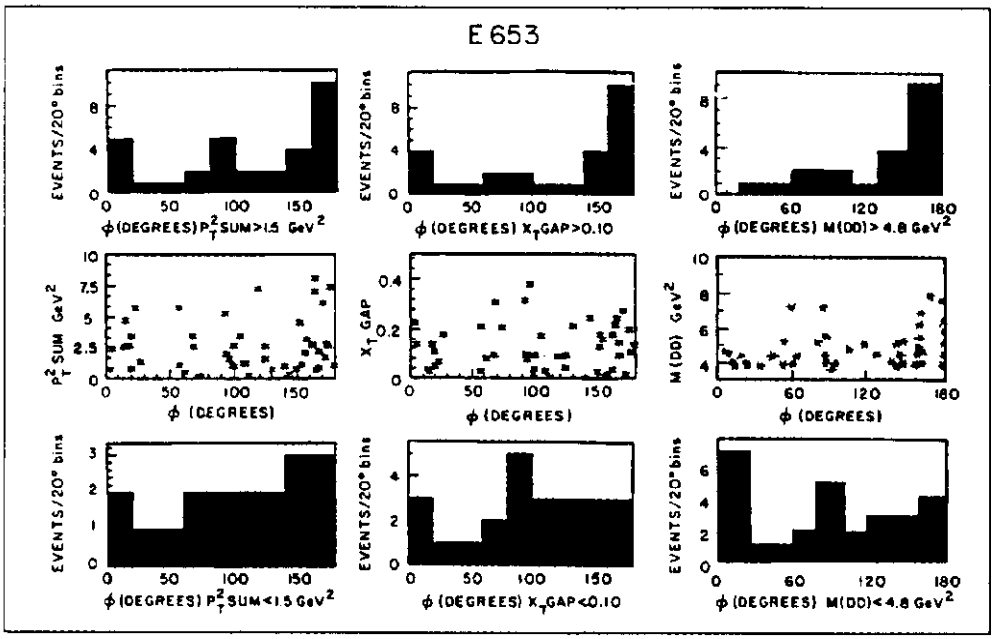

Figure 8. E653 data on correlations in the transverse plane vs production parameters, showing increased correlations with increased sum p_t of the charm pair, x_F gap between them and effective mass of the charm pair.

e+e- collisions. Their sample and our general understanding are not adequate yet to determine absolute branching ratios for D_s and charm baryons.

Theoretical work has been limited to leading order QCD calculations so far (69). However, Mangano, Nason and Ridolfi (70) have performed calculations which are relevant to collider energies and indicated ongoing work about to be available which will be relevant for fixed target experiments.

One should not leave the charm pair observations without noting the 1% fraction, relative to charm pair events, of double associated charm (i.e., 4 charm particles per event) reported by WA75 (71).

8. NUCLEAR TARGET DEPENDENCE

The use of small, solid targets is required in order to benefit from solid state tracking devices. This, in turn, necessarily raises the issue of the dependence of results on the nuclear material used. Not only is this important for comparing results among experiments with different targets, but also in extrapolating to

experiments with hydrogen targets and to theoretical calculations of the basic process. More fundamentally, if the process of producing charm quarks is truly the result of hard parton-parton interactions, one anticipates that the cross section will be proportional to the number of partons and, therefore, the number of nucleons in the target material, i.e. $\alpha=1$ in Equation 5.

$$\sigma = \sigma_0 A^{\alpha} \tag{5}$$

This is unlike diffractive production, for example, which should go as the atomic weight, A, to the 2/3 power. Thus, the A-dependence is a measure of the applicability of the QCD calculations. In fact, the early (indirect) measurements by WA78 (72, 73) and E613 (74) indicated a cross section which was proportional to $A^{3/4}$. This contributed to the belief that charm hadroproduction was not a domain where perturbative QCD calculations could be applied. There is also the possibility that the structure functions and fragmentation could vary with the nuclear environment.

The A-dependence of charm production is best measured by using directly observed charm particles in data taken in a single experiment from a variety of target materials at the same time. Both WA82 at CERN and E769 at Fermilab

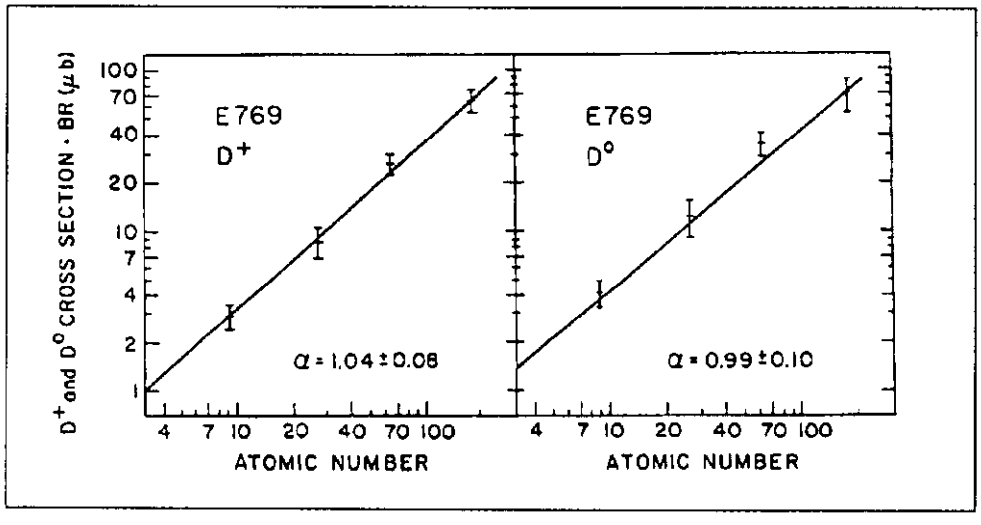

Figure 9. Nuclear target dependence of the D meson cross sections from E769.

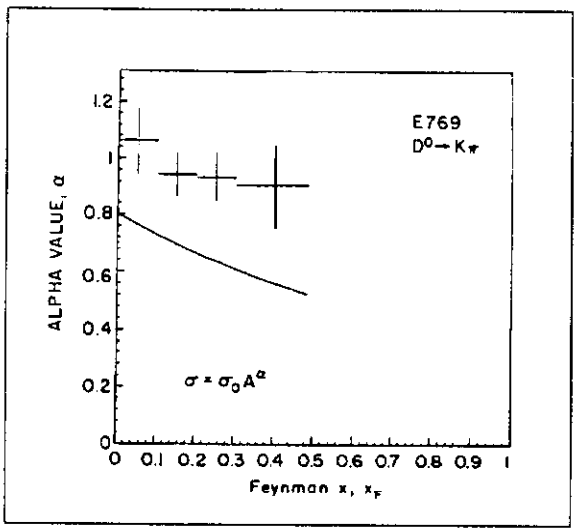

Figure 10. Dependence of the slope parameter a from figure 9 vs the scaled longitudinal momentum. The solid curve is from Barton, et al (75) and summarizes lower mass non-charm meson and baryon data.

followed this technique. Many experimental uncertainties cancel in the determination of α from the data. In E769, the beam went through all of the targets at the same time while in WA82, part of the beam went through each target material, providing less complete cancellation of the systematic errors and requiring knowledge of the beam profile and position. Data for D meson production from the four target materials of E769 (56) are shown in Figure 9. The parameterization of Equation 5 represents the data very well. Yet this and other recent results (Table 5) are inconsistent with the earlier indirect measurements.

Neither of the earlier measurements, by WA78 and E613, have significant x_F dependence in the plots in their papers. However, E613 described the result as "suggestive" of an x_F dependence. This may have been motivated by the well measured nuclear target dependence, for lower mass mesons and baryons, summarized by Barton et al (75). This possibility was supported in the review by

Table 5 A-Dependence charm data

Experiment	Process	α	x_F range	ref.
WA82	pA→D's	$0.88^{+0.04}_{-0.05}$	$0. < x_F > 0.7$	(57)
			$<x_F>=0.24$	
E769	$\pi A \rightarrow D^+$	1.04±0.08	$0. < x_F < 0.5$	(56)
	$\pi A \rightarrow D^0$	0.99±0.10	$0. < x_F < 0.5$	(56)
WA78	π-yield of prompt single μ^+	0.76±0.08	$< x_F > = 0.2$	(72)
	π-yield of prompt single μ^-	0.83±0.06	$< x_F > = 0.2$	(72)
	p yield of prompt single μ^+	0.79±0.12	$< x_F > = 0.1$	(73)
	p yield of prompt single μ^-	0.76±0.13	$< x_F > = 0.1$	(73)
E613	p prompt ν_e event rates	0.75±.0.05	$< x_F > = 0.15$	(74)

Tavernier (5). However, the most recent data do not support this suggestion (Figure 10) even though the data cover the same x_F range (76). In trying to explain the differences in the experimental results, it is easiest to imagine changes in experimental conditions during the different target configurations used in the beam dump experiments e.g., the beam halo or other instrumental effects. In any event, the systematic uncertainties are inherently smaller in the more recent data.

The very high statistics measurements of A-dependence for the production of hidden charm in the hadroproduction of the J/ψ and ψ' (77) gave an α value of 0.920 ± 0.008. If outgoing charm quarks felt only small nuclear effects, one could imagine that the open charm and hidden charm A-dependence would be the same. At this point, the data are consistent with this view. Higher statistics yet will be needed for the open charm for better A-dependence measurements as a function of x_F and p_t. It will be interesting to compare these dependences with those observed for the J/ψ.

The motivation for developing theoretical models to explain an A-dependence that is different from $\alpha = 1$ is greatly reduced by the recent data. Nevertheless, deviations from $\alpha = 1$ may be due to absorption of the incident hadrons (78), changes in the gluon structure functions as a function of the nuclear environment (79) or color screening effects on the outgoing charm quark matter (80). The recent references cited find it difficult to explain large deviations from $\alpha = 1$.

9. SUMMARY AND OUTLOOK

Charm hadroproduction is in the midst of its second generation of work in both experiment and theory. This is a high productivity generation, one with high statistics, open acceptance and good signal/background ratios from experiments and a consistent theoretical picture based on quantum chromodynamics calculated to next to leading order. Progress in experimental technique beyond the first generation has been dependent on precision tracking of charged particles in a very large sample of fixed target data. That data are in general, even quantitative,

accord with QCD predictions. The predictions are based on the dominance of the gluon-gluon fusion process, but require detailed and quantitative understanding of the next to leading order QCD processes.

There is no continuing evidence for the earlier large effects which were not easily explained in QCD models. Recent data do not show steep energy dependence of the cross section, nor large leading particle production nor intrinsic charm in nucleons.

There is evidence for similarity in the gluon structure functions in pions and kaons, and softer gluon distributions in protons. The fragmentation process where charm quarks turn into outgoing hadrons appears to be very hard, i.e., the charm particle taking essentially all the energy of the initial charm quark. The hadronization process remains to be fully explained; even the Monte Carlo methods have not yet been tuned to match hadronization data.

The most recent measurements of nuclear target dependence also encourage a QCD interpretation of the production process. Earlier indirect measurements have been supplanted by higher statistics direct measurements which indicate a cross section nearly proportional to the number of nucleons in the target as anticipated for constituent hard scattering processes.

As of the time of this review, final results from the high statistics experiments which took data at the end of the 1980's are just appearing. Yet to come are the detailed interpretations of these data and the results of even higher statistics data already taken in the decade of the 1990's. New techniques to further exploit the power of solid state detectors used for precision tracking are needed for any major leap in capability for hadroproduction of charm experiments. Such improvements would be useful in both selecting charm events and increasing the recording of interesting events. Any improvement is likely to affect both at the same time. While progress is being made, the technologies are both expensive and time consuming to develop. Such improvements, as well as a new kinematic regime of hadroproduction data, may come from hadron collider experiments where the

high energy physics community is focusing much more money and effort. In the mean time, charm hadroproduction is enjoying a period rich in data and providing an opportunity for detailed comparisons with theory, a period which should see increases in both basic understanding and quantitative parameterization.

10. ACKNOWLEDGMENTS

I gratefully acknowledge my colleagues on the series of charm experiments at the Fermilab Tagged Photon Laboratory for enlightening discussions over the many years of work there, and recently, especially to Paul Karchin, Robert Jedicke, Simon Kwan, and Jeff Spalding. I also acknowledge Leonardo Rossi for discussions of recent CERN data and Keith Ellis for explaining many theoretical points. Thanks go to Sudeshna Banerjee, Tom Carter, Austin Napeir, Jean Slaughter and Keith Thorne for help with this article, and to Kristen Ford for her extra effort and for expertly preparing this manuscript.

Work on this review was supported by the U.S. Department of Energy under contract No. DE-AC02-76CHO3000.

11. LITERATURE CITED

1. Glashow, S. L., Iliopoulos, J., Maiani, L., Phys. Rev. D2: 1285 (1970)
2. Aubert, J. J., et al., Phys. Rev. Lett. 33: 1404 (1974)
3. Augustin, J. E., et al., Phys. Rev. Lett. 33: 233 (1975)
4. Kernan, A., VanDalen, G., Physics Reports, 106: 297 (1984)
5. Tavernier, S. P. K., Rep. Prog. Phys. 50: 1439 (1987)
6. Brodsky, S. J., Hoyer, P., Peterson, C. Sakai, N., Phys. Lett. 93B: 451 (1980); Brodsky, S. J., Peterson, C., Sakai, N., Phys. Rev. D23: 2745 (1981); Bertsch, G., Brodsky, S. J., Goldhaber, A. S., Gunion, J. F., Phys Rev. Lett. 47: 297 (1981)
7. Combridge, B. L., Nucl. Phys. B151: 429 (1979)
8. Odorico, R., Nucl. Phys. B209: 77 (1982)
9. Fritzsch, H., Streng, K. H., Phys. Lett. 78B: 447 (1978)
   Halzen, F., Keung, W. -Y., Scott, D. M., Phys Rev D 1631: 28 (1983)
10. Likhoded, A. K., Slabospitskii, S. R., Suslov, M. V., Sov. J. Nucl. Phys. 38: 433 (1983)
    Roy, D. P., Desai, B. R., Z. Phys. C 22: 149 (1984)
    Cooke, M. A. L., Z. Phys. C 26: 71 (1984)
    Brodsky, S. J., Gunion, J. F., Soper, D. E., Phys. Rev. D 36: 2710 (1987)
11. Nason, P., Dawson, S., Ellis, R. K., Nucl. Phys. B303: 607 (1988)
12. Aguilar-Benitez, M., et al., Nucl. Instrum. Methods A258: 26 (1987)
13. Ammar, R., et al., Phys. Lett. B183: 110 (1986)
14. Aoki, S., et al., Phys. Lett. B 187: 185 (1987)
15. Kodama, K., et al., Nucl. Instrum. Methods A289: 146 (1990)
16. Bailey, R., et al., Z. Phys. C 30: 51 (1986)
17. Bailey, R., et al., Z. Phys. C 28: 357 (1985)
18. Bailey, R., et al., Nucl. Instrum. Methods 213:201 (1983)
19. Adamovich, M., et al., Nucl. Instrum. Methods A309: 401 (1991)
20. Raab, J. R., et al., Phys Rev D 37: 2391 (1988)

21. Appel, J. A., Proc. Europhysics Study Conference on High-Energy Physics, Erice, Sicily, Italy, 555 (1981)
22. Damerell, C., et al., Comput. Phys. Commun. 22: 349 (1982)
23. Daum, C., et al., Nucl. Instrum. Meth. 217: 361 (1983)
24. Anthonioz-Blanc, J., et al., CERN-DD/80/14 CERN (1980)
Adamovich, M., et al., IEEE Trans. Nucl. Sci. 37: 236 (1990)
25. Nash, T., Computing and High Energy Physics Conf., Tsukuba, Japan, FERMILAB-CONF-91-87 (1991)
26. Haber, C., et al., Nucl. Instrum. Methods A289: 388 (1990)
27. Ikeda, M., et al., Proceedings of the 8th Topical Workshop on Proton-Antiproton Collider Physics, Castigilione, Italy, 558 (1989)
28. Abe, F., et al., Phys. Rev. Lett. 64: 348 (1990)
29. Arnison, G., et al., Phys. Lett. 147B: 222 (1984)
30. Fisher, C. M., Proc. Photonics Applied to Nuclear Physics, Strasbourg, 92 (1981)
Harigel, G. G., Nucl. Instrum. Methods A257: 614 (1987); Harigel, G. G., Nucl. Instrum. Methods A279: 249 (1989)
31. Majka, R. D., et al., IEEE Trans. Nucl. Sci. 36: 63 (1989)
Sandweiss, J., et al., Phys. Rev. Lett. 44: 1104 (1980)
Eckardt, V., Wenig, S., Nucl. Instrum. Methods 213: 217 (1983)
32. Angelini, C., et al., Nucl. Instrum. Methods A289: 342 (1990)
Ruchti, R., et al., IEEE Transactions on Nuclear Science 35: 441 (1988)
33. Amendolia, S. R., el al., Nucl. Instrum. Methods 226: 78 (1984)
Coteus, P., et al., IEEE Transactions on Nuclear Science 32: 585 (1984)
Barlag, S. et al., Z. Phys. C 37: 17 (1987)
34. Shapiro, S., et al., Nucl. Instrum. Methods A257: 580 (1989); Gaalema, S., et al., Proc. Int. Industrial Symposium on the Supercollider, New Orleans, LA, 173 (1989)
Anghinolfi, F., et al., CERN/ECP 91-26 CERN (1991)
Parker, S., et al., Nucl. Instr. Methods A275: 494 (1989)
Heinemann, B., et al., Nucl. Instr. Methods A305: 517 (1991)

35. Gluck, M., Owens, J. F., Reya, E., Phys. Rev. D17: 2324 (1978); Combridge, B. L., Nucl. Phys. B151: 429 (1979)
36. Collins, J. C., Soper,D. E., Sterman, G., Nucl. Phys. 263B: 37 (1986)
37. Nason, P., Dawson, S., Ellis, R. K., Nucl. Phys. B327: 49 (1989)
38. Beenakker, W., et al., Phys. Rev. D40: 54 (1989); Beenakker, W., et al., Nucl. Phys. B351: 507 (1991)
39. Berger, E., Workshop on Physics at Fermilab in the 1990's Breckenridge, Colorado, 70 (1989) with additional data from (50) and (55)
40. Sjöstrand, T., International Journal of Modern Physics A3: 751 (1988)
41. Paige, F. E., Protopopescu, S. D., Proc. of the 1986 Summer Study on thePhysics of the Superconducting Super Collider, Snowmass, CO, 320 (1986)
42. Bengtsson, H. -U., Sjöstrand, T., Computer Phys. Comm. 46: 43 (1987)
43. Ali, A., van Eijk, B., ten Have, I., Nucl. Phys. B292: 1 (1987)
44. Field, R. D., Feynman, R. P., Nucl. Phys. B136: 1 (1978)
45. Andersson, B., Gustafson, G., Nilsson-Almqvist, B., Nucl Phys. B281: 289 (1987); Nilson-Almqvist, B., Stenlund, E., Computer Phys. Comm. 43: 387 (1987)
46. Barlag, S., et al., Z. Phys. C. 49: 555 (1991)
47. Barlag, S., et al., Phys. Lett. B 247: 113 (1990)
48. Barlag, S., et al., Phys. Lett. 236: 495 (1990)
49. Barlag, S., et al., Phys. Lett. 233: 522 (1989)
50. Wu, Z., Ph. D. Dissertation, Yale University, New Haven, Ct., USA (unpublished) (1991)
51. Jedicke, R., Ph.D. Dissertation, University of Toronto, Toronto, Canada (unpublished) (1991)
52. Barlag, S., et al., Z. Phys. C 39: 451 (1988)
53. Kodama, K., et al., Phys. Lett. B 263: 573 (1991)
54. Gunion, J. F., Phys. Lett. 88B: 150 (1979)
55. Aguilar-Benitez, M., et al., Nucl. Phys. B161: 400 (1985)

56. Gay, C. W., Ph.D. Dissertation, University of Toronto, Toronto, Canada (unpublished) (1991)
57. de Mello Neto, J. T., Ph.D. Dissertation, Centro Brasileiro de Pesquisas Fisicas, Rio de Janeiro, Brazil (unpublished) (1992)
58. Adamovich, M., CERN-PRE-91-095
59. Adamovich, M. I., et al., CERN-EP/89-123
60. Aguilar-Benitez, M., et al., Z. Phys. C 40: 321 (1988)
61. Ammar, R., et al., Phys. Rev. Lett. 61: 2185 (1988)
62. Aguilar-Benitez, M., et al., Phys. Lett. 164B: 404 (1985)
63. Aguilar-Benitez, M., Z. Phys. C 40: 321 (1988)
64. Aoki, S., et al., Phys. Lett. B 209: 113 (1988)
65. Kodama, K., et al., Phys. Lett. B 263: 579 (1991)
66. Barlag, S., et al., Phys. Lett. B 257: 519 (1991)
67. Kodama, K., et al., CMU-HEP91-18 (1991)
68. Barlag, S., et al., Z Phys. Lett. C48: 29 (1990)
69. Kunszt, Z., Pietarinen, E., Nucl. Phys. B164: 45 (1980); Kunszt, Z., Gunion, J. F., Phys. Lett. 178B:296 (1986); Ellis, R. K., Sexton, J. C., Nucl. Phys. B269: 445 (1986)
70. Mangano, M., Nason, P., Ridolfi, G., GEF-th-10/1991 and UPRF-91-308
71. Aoki, S., et al., Phys. Lett. B 187: 185 (1987)
72. Cobbaert, H., et al., Phys. Lett. B 191: 456 (1987)
73. Cobbaert, H., et al., Phys. Lett. B 206: 546 (1988)
74. Duffy, M. E., et al., Phys. Rev. Lett. 55: 1816 (1985)
75. Barton, D. S., et al., Phys. Rev. D 27: 2580 (1983)
76. Alves, G., PhD. Dissertation, Centro Brasileiro de Pesquisas Fisicas, Rio de Janeiro, Brazil (unpublished) (1992)
77. Alde, D. M., et al., Phys. Rev. Lett. 66: 133 (1991)
78. Gavin, S., Gyulassy, M., Phys. Lett. B 214: 241 (1988)
79. Close, F. E., Qiu, J., Roberts, R. G., Phys. Rev. D 40: 2820 (1989)
Aubert, J. J., et al., Phys. Lett. 152B: 433 (1985)
Sokoloff, M. D., et al., Phys. Rev. Lett. 57: 3003 (1986)

80. Mueller, A., Proc. of the XVII Recontre de Moriond, ed. Tran Thanh Van, J., Editions Frontieres, Gif-sur-Yvette, France, 13 (1982); Brodsky, S. J., Proc. of the XIII Int. Symp. on Multiparticle Dynamics, eds. Kittel, W., Metzger, W, and Stergiou, A., World Scientific, Singapore, 963 (1983)
Appel, J. A., Botts, J., Bunce, G., Farrar, G., Pordes, S., BNL-45319, Brookhaven, NY; Proceedings for DPF Summer Study, Snowmass, CO (1990)